Chapter 6

Resultant Residual Stresses due to The Full Coupling of Phase Transformation, Thermal Loading and Mechanical Loading

6.1 Onset of Irreversible Deformation

The term thermal critical grinding conditions means the combined thermal and mechanical grinding conditions required to initiate plastic deformation in the workpiece at steady-state loading. To understand the mechanism of irreversible deformation, the stress field associated with given grinding parameters needs to be explored. For an elastic material with constant thermal and mechanical properties the stress solution due to the mechanical load and the thermal load can be superimposed to yield thermo-mechanical effective stress. Figure 6.1 investigated the stress field associated with different grinding conditions. The effective stress curves show sharp gradients at some points near the workpiece surface. It is clear that maximum effective stress can be developed at different locations relative to the surface loading position. There exists a local maximum effective stress zone near the surface of the workpiece. In contrast to the iso-thermal stress conditions illustrated in Fig. 5.3, maximum effective stress can occur at the workpiece surface (Fig. 6.1a,b). Moreover the stress gradient of the local maximum effective stress near the workpiece surface is the highest among those within the workmaterial. The location of the maximum effective stress contours indicate that plastic deformation always starts within the grinding zone which in turn influences the distribution of the residual stresses developed at the earliest stage. The onset location of plastic deformation is very sensitive to thermal and mechanical load combinations particularly at a high critical heat flux intensity (Fig. 6.1b,c). However, it will move from the surface to a deeper layer when mechanical normal traction increases.

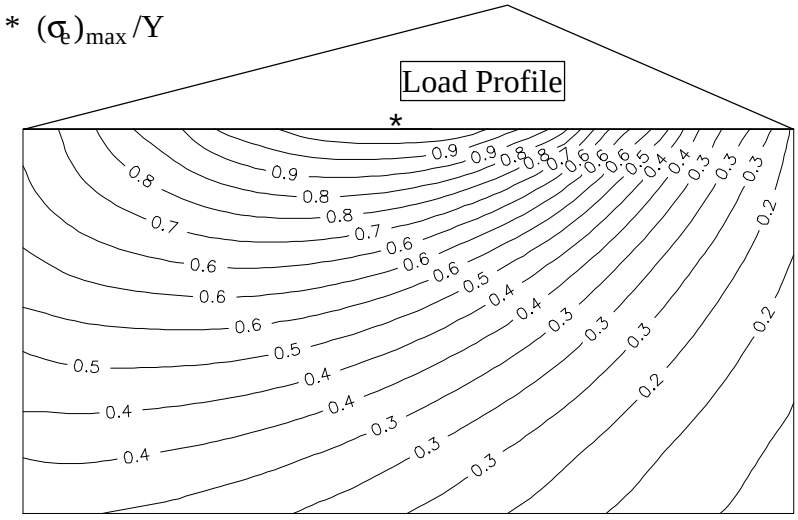

(a) $p_a/Y=0.0$, $q_a=12.333$ MW/m^2, H=0, Pe=1, $l_a=0.25$

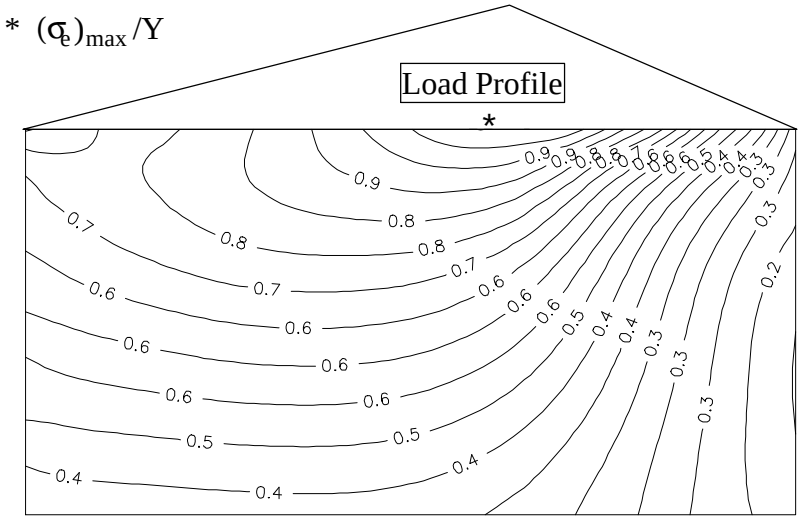

(b) $p_a/Y=0.4$, $q_a=12.834$ MW/m^2, H=0, Pe=1, $l_a= 0.25$ $\mu=0.1$

Figure 6.1 Critical Thermo-mechanical effective stress to yield stress ratio field

To investigate critical thermo-mechanical grinding conditions, a large number of case studies is examined in Fig. 6.2. A typical condition of up-grinding ($l_a=0.25$) is analyzed by varying the input heat flux intensity, q_a, the convection heat transfer coefficient, H, the

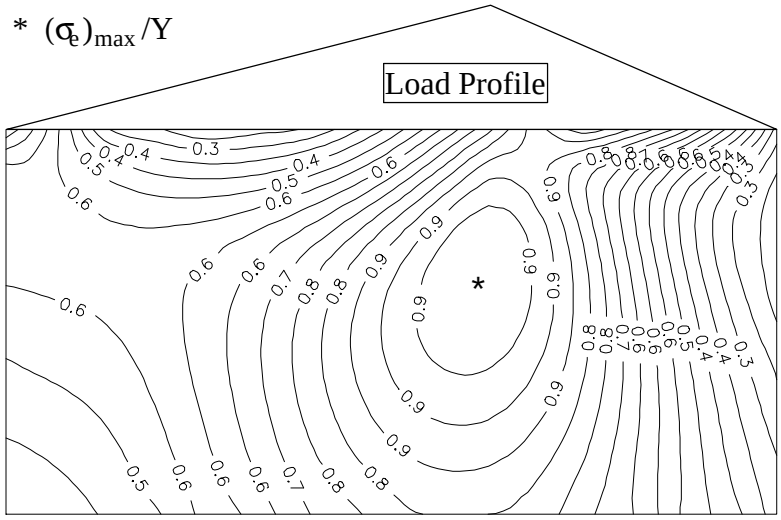

(c) $p_a/Y=1.0$, $q_a=15.846$ MW/m^2, H=0, Pe=1, $l_a=0.25$ $\mu=0.1$

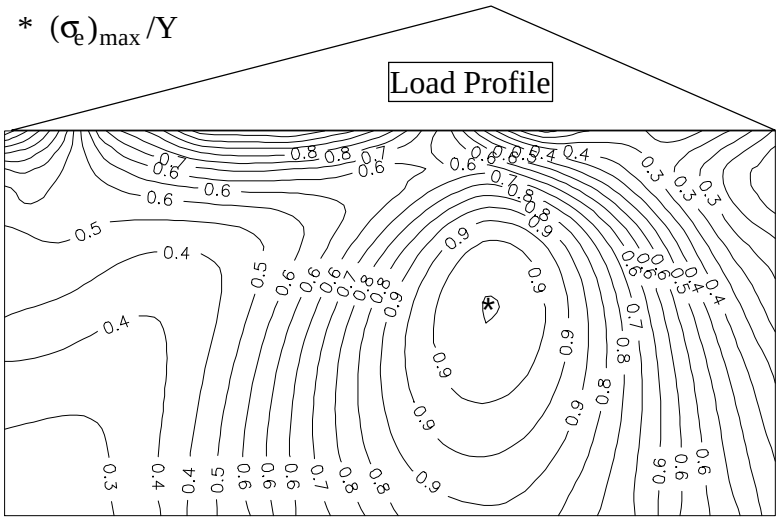

(d) $p_a/Y=1.08$, $q_a=1.515$ MW/m^2, H=0, Pe=1, $l_a=0.25$ $\mu=0.1$

Figure 6.1 Critical Thermo-mechanical effective stress to yield stress ratio field (continued)

Peclet number, Pe, the peak of the mechanical normal traction, p_a μ. It

intensity, q_a, and the normal traction pressure, p_a (see Fig. 6.2a). The critical heat flux

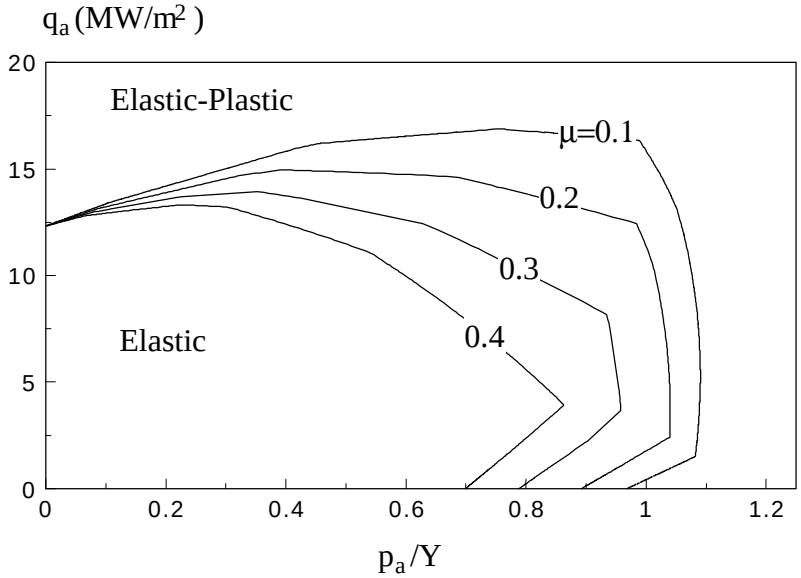

(a) effect of 'friction' factor (H=0, Pe=1)

Figure 6.2 Critical Thermomechanical grinding (l_a=0.25)

intensity, q_a, increases as traction rises to a maximum near p_a/Y= 0.2 after that the critical heat

that a higher friction factor results in a lower critical traction intensity. It is interesting to note that plastic deformation may be developed at a lower heat flux intensity (q_a < 5 MW/m^2) but with high levels of normal traction. The reason behind the complex behaviour of the critical heat flux intensity conditions for high traction is related to the different associated stress fields and the corresponding local maximum effective stress locations. On the other hand, the convection heat transfer coefficient, H, has a reversed role in critical grinding conditions as a higher convection heat transfer coefficient requires higher levels of critical heat flux intensity and normal traction pressure (see Fig. 6.2b) to meet the same grinding temperature as above. It is clear that more heat flux intensity is needed to maintain initial plastic deformation as grinding temperature decreases. Moreover, the critical heat flux intensity is proportional to the normal traction pressure profile to a limit characterized by sudden decrease of the critical heat flux intensity at about p_a/Y=1.1 for H=1.0.

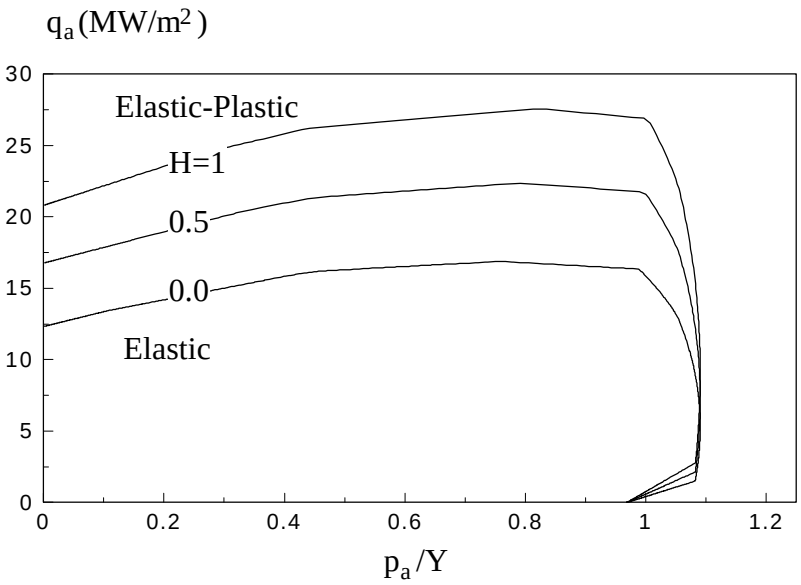

(b) effect of convection heat transfer coefficent (Pe=1,μ=0.1)

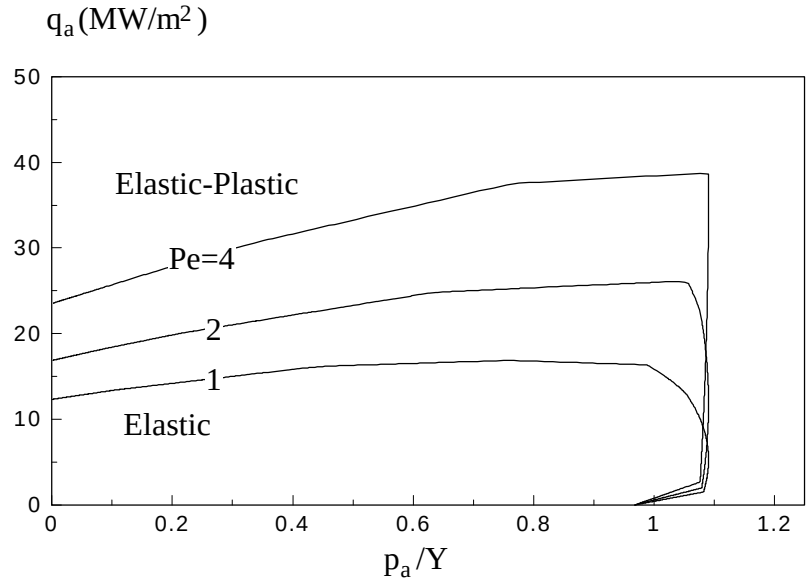

(c) effect of Pecklet number (H=0, μ=0.1)

Figure 6.2 Critical Thermomechanical grinding conditions (l_a=0.25) (continued)

Table speed has a similar role to that of the convection heat transfer coefficient since a higher table speed results in a lower grinding temperature if heat flux intensity is kept the same. Therefore higher Peclet numbers result in higher levels of critical heat flux intensity to a limit of p_a/Y=1.1.

6.2 Grinding Stress History

During the grinding process the workpiece is subjected to moving thermal and mechanical loads with their magnitudes relying on the grinding conditions. This will result in irregular thermal and mechanical deformations in the ground surface which in turn lead to a complex stress field history. Therefore, it is important to trace the grinding stress history in terms of loading conditions and workmaterial properties. It should be noted that all the following grinding conditions are limited by the fact that they are transient in nature.

6.2.2 Grinding Surface Strain History

Figure 6.3 demonstrates the thermal and mechanical longitudinal strain, ε_{xx}, in relation to the location of the moving load at the workpiece surface. It is found that strains approach their steady state conditions shortly after a few load movement steps. Under thermal loading conditions of grinding, the ground surface exhibits compressive strain in front of the thermal load followed by rapid increase of tensile strain. (Fig. 6.3a). The thermal strain history indicates that as the grinding zone is heated it tries to expand but is restricted by the zone ahead, which is experiencing a lower temperature rise, so that a compressive stress forms. The iso-thermal mechanical loading conditions, on the other hand, result in a local compressing strain with a sharp gradient away from the grinding zone. This is obvious as surface traction presses the ground surface of the grinding zone. A stretched surface is developed after mechanical load movement which is similar to the results under thermal loading (see Fig. 6.3b). Figure 6.3c presents the effect of the combined thermo-mechanical loading. The combination of thermal and mechanical loading shows a somewhat intermediate state of strain with similar trends to that of thermal grinding conditions but with more compressive strains.

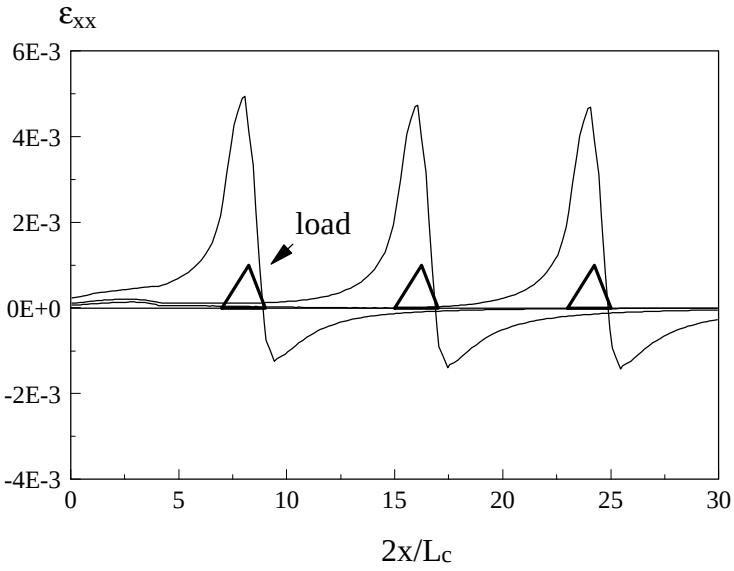

(a) thermal load only (q_a =43.25 MW/m^2 ,Pe=1,H=1)

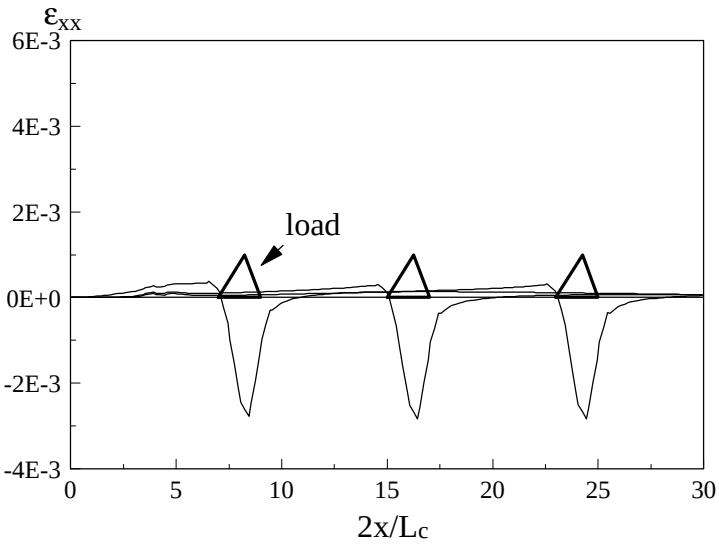

(b) mechanical load only (p_a /Y=2, μ=0.1)

Figure 6.3 Strain history and load movements (l_a=0.25)

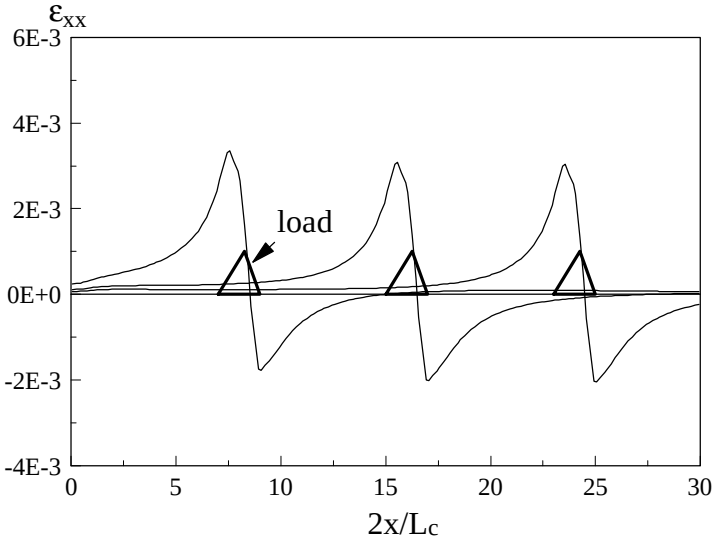

(c) thermomechanical load
(p_a /Y=2, μ=0.1, H=1, Pe=1,q_a=43.25 MW/m²)

Figure 6.3 Strain history and load movements (l_a=0.25) (continued)

6.2.2 Grinding Surface Stress History

The stress history corresponding to the above mentioned typical grinding conditions is discussed in Fig. 6.4. Figure 6.4a shows that the history of longitudinal thermal surface stress, σ_{xx}, is characterized by an initial growing compressive stress followed by a progressing tensile stress. The remaining stress is of tensile nature. If the mechanical load is superimposed (see Fig. 6.4b) on the thermal loading, the remaining stress vanishes which indicates that the effect of mechanical traction eliminates that of thermal loading and therefore makes the maximum effective stress below yield stress. On the other hand, when the maximum grinding temperature is maintained at the same level, the Peclet number must become four times higher under dry grinding conditions as illustrated in Fig. 6.4c. When compared with the results of Fig 6.4a, a tensile longitudinal stress history is obtained. All these indicate that grinding stress development is sensitive to some thermal and mechanical conditions.

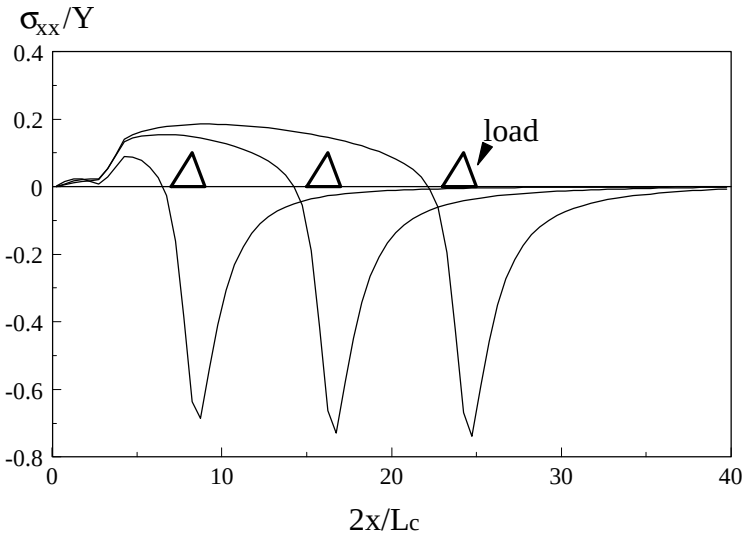

(a) (l_a=0.25, H=1, Pe=1, q_a=43.25 MW/m^2)

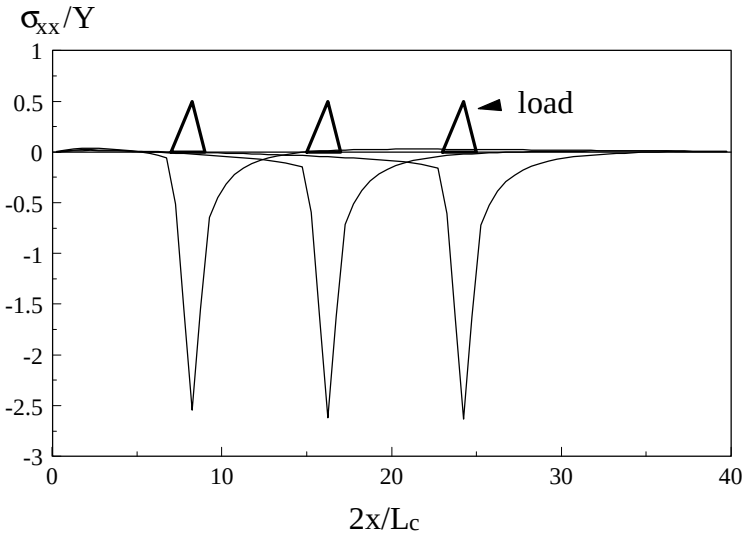

(b) (l_a=0.25, H=1, Pe=1, q_a=43.25 MW/m^2 , p_a /Y=2, μ= 0.1)

Figure 6.4 Grinding stresses history

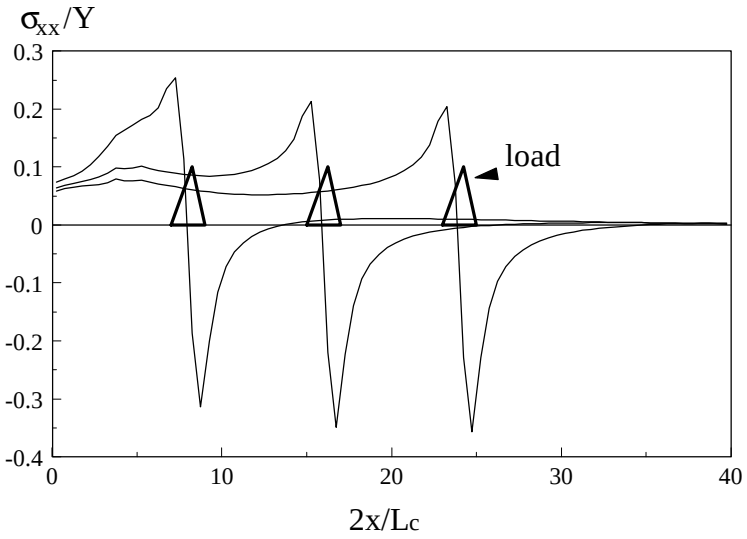

(c) (l_a=0.25, H=0, Pe=4, q_a=47.25 MW/m^2 , p_a/Y=2, μ= 0.1)

Figure 6.4 Grinding stresses history (continued)

6.3 Thermo-Mechanical Residual Stresses

There are two major surface residual stresses, σ_{xx} and σ_{yy}, and the magnitudes of these are directly related to the grinding conditions. A comparison with experimental results shows that the nature of the thermo-mechanical residual stresses of an up-grinding (l_a=0.25) (present study) is in agreement with that of Ramanath and Shaw (1986) (see Fig. 6.5) where they used $Al_3 O_2$ wheel. The surface tensile stresses in the direction of grinding increases with depth to a certain extent and then decreases. The depth of the residual stresses of their experimental results is smaller than the present theoretical prediction. This can be attributed to the main assumption made about the continuous contact traction. In other words, the experimental results are based on a discrete contact that is much smaller than the present grinding zone length.

As shown in Fig. 6.6, greater traction may decrease the magnitudes of both the residual stresses if the ratio of the horizontal to vertical traction is low (e.g., $|\mu| = 0.1$). This is attributed to the relaxation of the initial surface compressive stresses generated by heating in the grinding zone, which in turn reduces the total longitudinal strain and the surface stresses. For a high μ (e.g., 0.3), a greater surface traction would lead to an undesirable residual stress distribution (see

Figs. 6.6e,f). This is because the surface workmaterial in the grinding zone experienced a greater initial surface stretching and thus a larger tensile stress, σ_{xx}, during grinding. In this sense, therefore, an up-grinding operation is advantageous in terms of residual stresses if a lower heat flux input and a smaller μ can be maintained.

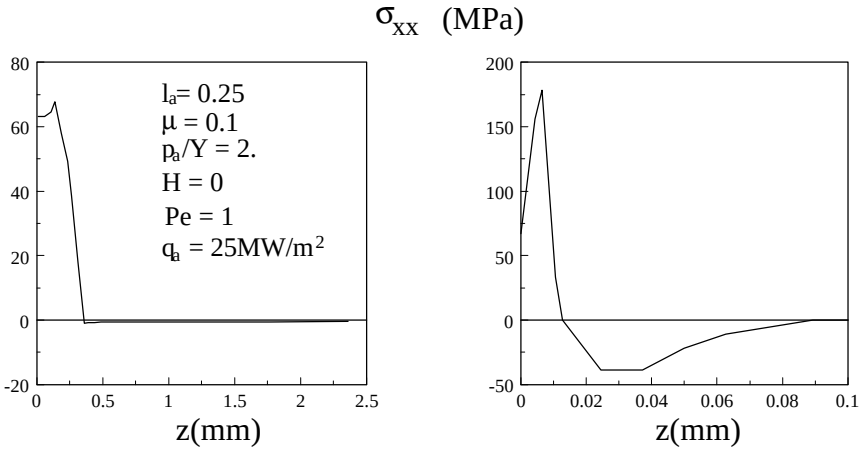

(a) workmaterial EN23 steel, thermo mechanical grinding conditions (present study)

(b) workmaterial case carburised steel, air cooling, Al_2O_3 wheel, v_{wh} =32m/sec, d_c = 0.012 mm, v = 0.14 m/sec (Ramanath and Shaw (1986))

Figure 6.5 Grinding residual

Figure 6.7 indicates that a down-grinding mechanism introduces smaller surface residual stresses if the peak of the vertical surface traction is below the yield stress of the workmaterial, i.e., if $p_a/Y < 1$. It is understandable as the thermal residual stresses must become dominant when $p_a/Y < 1$ and the grinding temperature associated with a down-grinding process is less than associated that with an up-grinding. If p_a is high (but $p_a/Y \leq 2$), however, an up-grinding results in less residual stresses and therefore is more favourable.

The increase of the heat flux intensity elevates the grinding temperature and in turn enlarges the thermal strains. It is apparent according to Figs. 6.7c-d that the coupling of

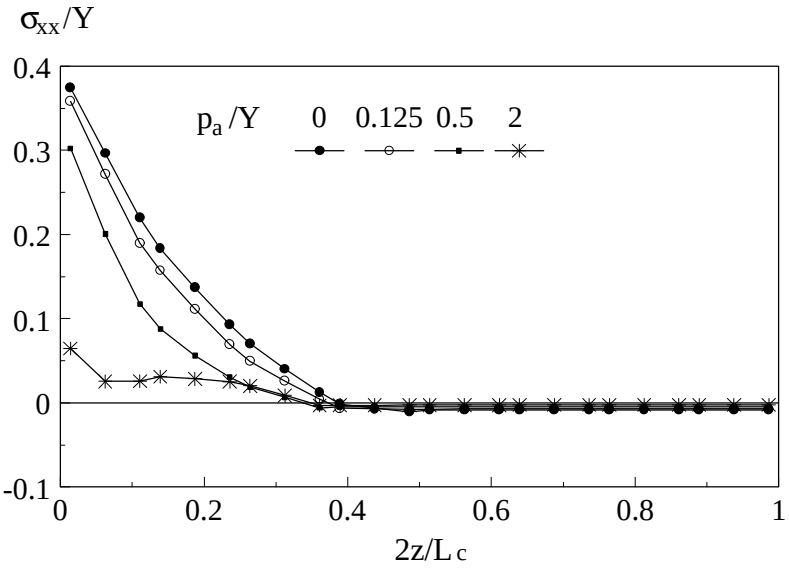

(a) σ_{xx}, (μ=0.1, l_a=0.25)

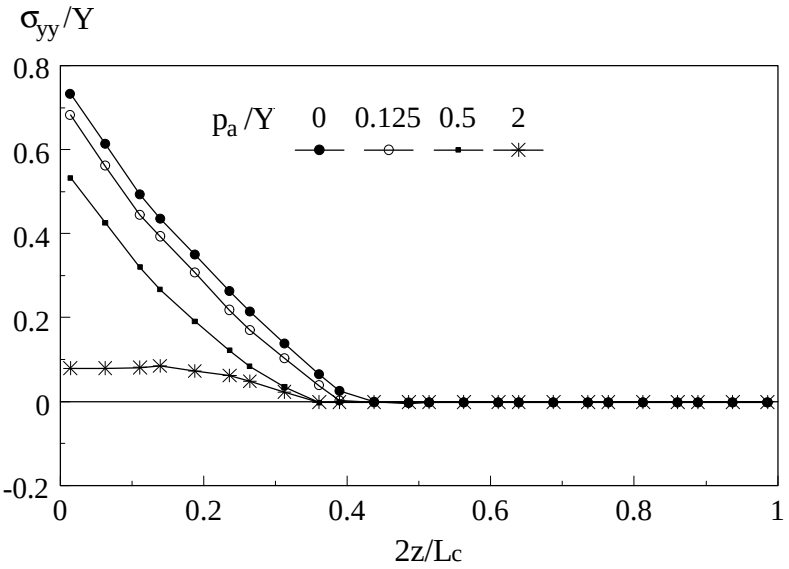

(b) σ_{yy}, (μ=0.1, l_a=0.25)

Fig. 6.6 Typical thermomechanical residual stress
(H=0, l_a=0.25, Pe=1, q_a=25 MW/m^2)

mechanical traction with a high input of heat flux has a similar effect to that of pure thermal loading conditions, because greater surface residual stresses are generated. It should be noted that the grinding temperature in down-grinding is lower so that down-grinding produces less residual stresses. This is similar to the results with smaller p_a/Y <1, as shown in Figs

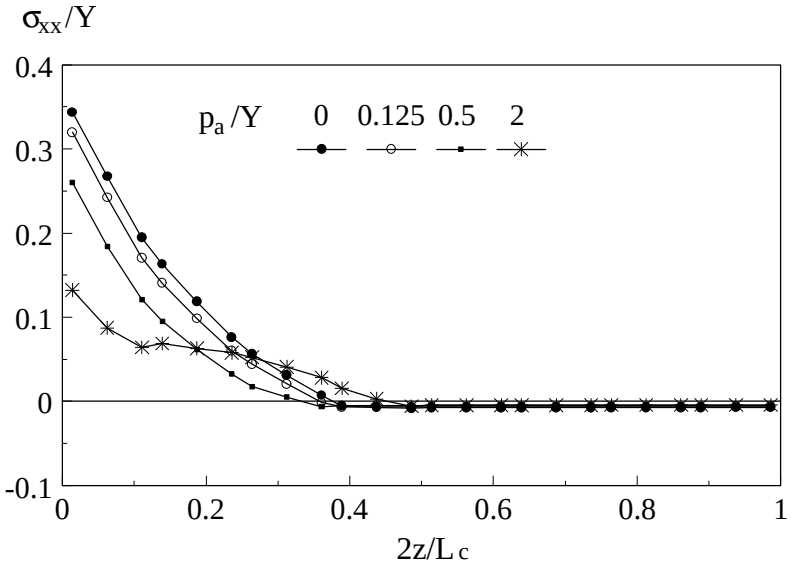

(c) σ_{xx}, (μ=0.1, l_a =0.75)

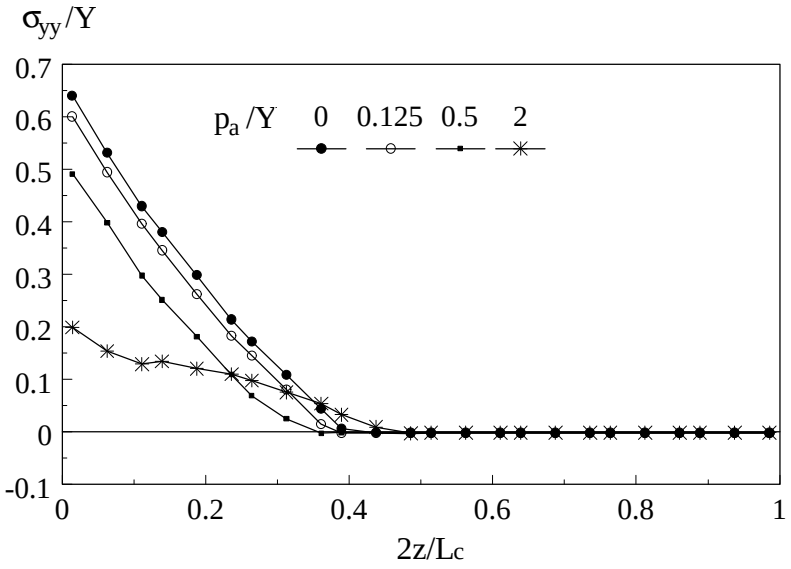

(d) σ_{yy}, (μ=0.1, l_a =0.75)

Fig. 6.6 Typical thermo-mechanical residual stress (H=0, l_a=0.25, Pe=1, q_a=25 MW/m^2) (continued)

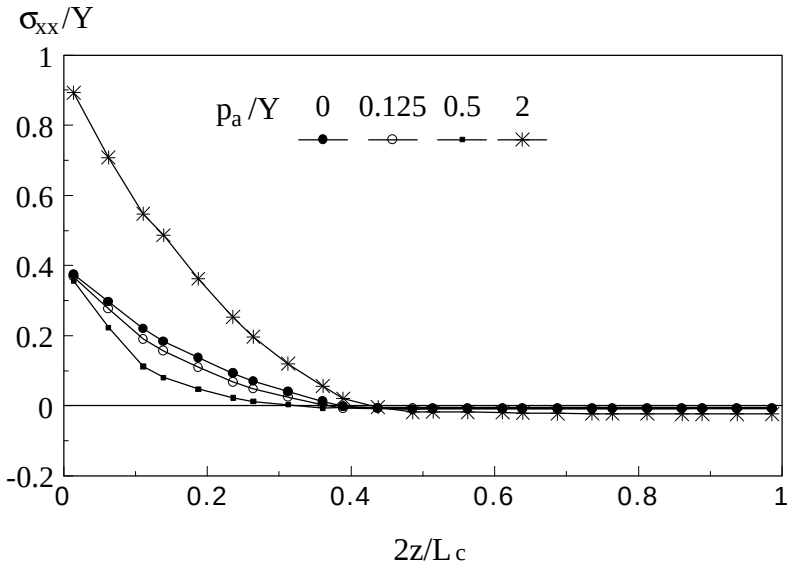

(e) σ_{xx}, (μ=0.3, l_a =0.75)

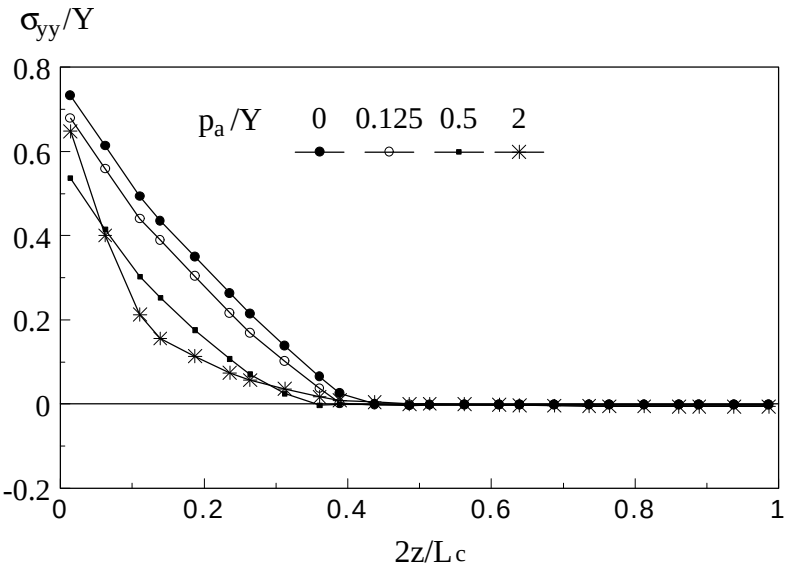

(f) σ_{yy}, (μ=0.3, l_a =0.75)

Fig. 6.6 Typical thermo-mechanical residual stress distribution (H=0, l_a=0.25, Pe=1, q_a=25 MW/m^2) (continued)

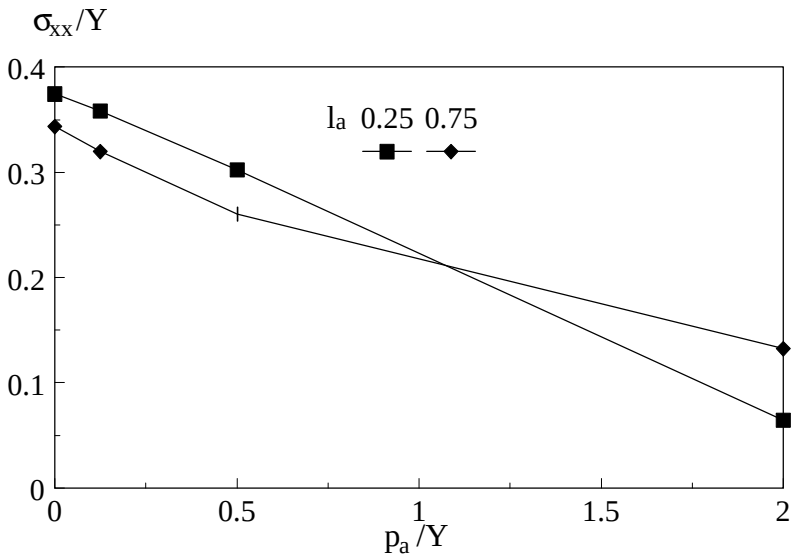

(a) σ_{xx}, (q_a =25 MW/m^2)

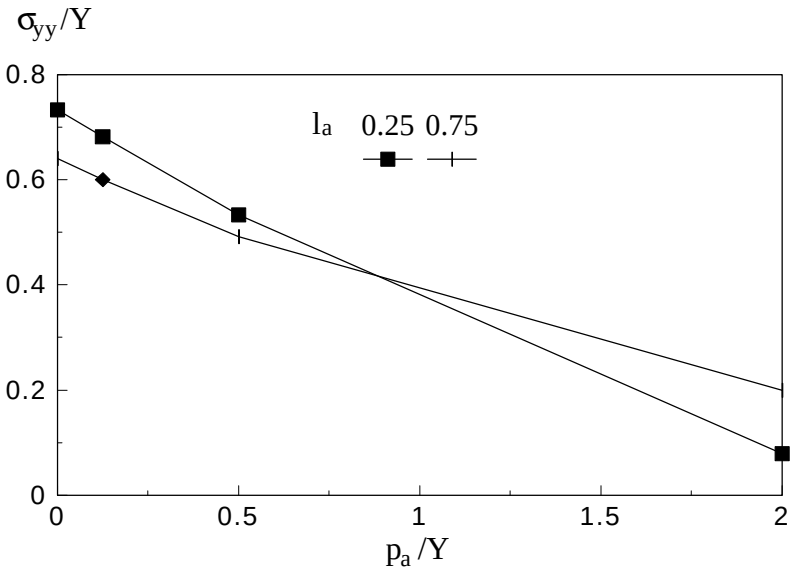

(b) σ_{yy}, (q_a =25 MW/m^2)

Fig. 6.7 Surface thermo-mechanical residual stresses and type of grinding (H =0, Pe =1.0, μ =0.1)

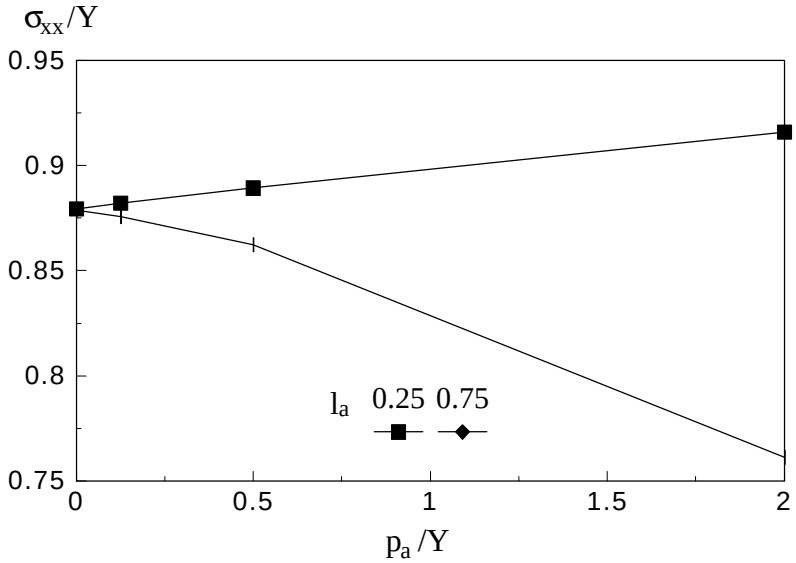

(c) σ_{xx}, (q_a =50 MW/m^2)

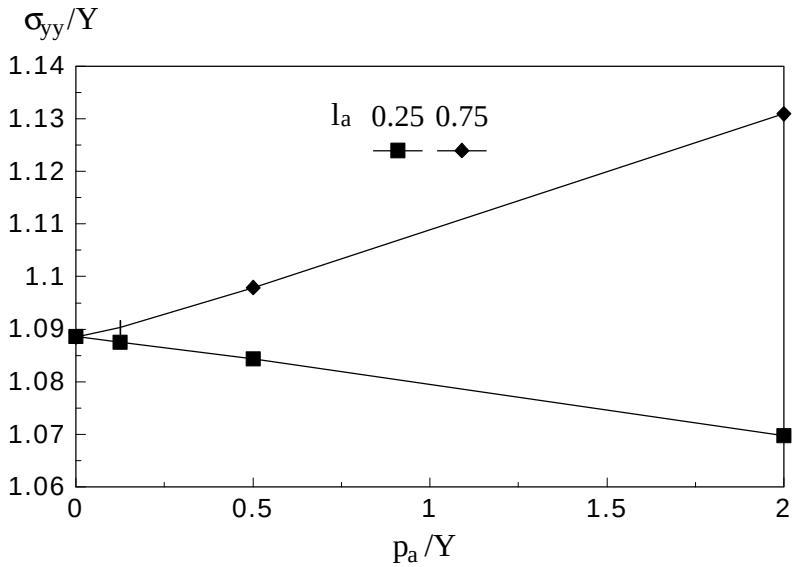

(d) σ_{yy}, (q_a =50 MW/m^2)

Fig. 6.7 Surface thermo-mechanical residual stresses and type of grinding (H=0, Pe =1.0, μ=0.1) (continued)

6.7a,b. In addition, the increase of mechanical traction increases longitudinal residual stress, σ_{xx}, but has little effect on plane residual stress, σ_{yy}.

Cooling due to grinding fluid has a remarkable effect on residual stresses. Figure 6.8 shows the results of an up-grinding process when the convection heat transfer coefficient, H, increases and when the maximum grinding temperature remains the same as in the case studies discussed above. The results indicate that a higher traction can decrease the residual stresses and even a state of no residual stresses can be achieved when $p_a/Y = 2$. The mechanism of such an interesting phenomenon can be elucidated when the stress variation in relation to the motion of surface traction is monitored. As shown in Fig. 6.9a, in the early stages of the traction motion, e.g., at $2x_c/L_c = 8$ where x_c is the coordinate of the traction centre, the longitudinal stress σ_{xx} is slightly tensile. With further movement of the traction the stress becomes compressive. The reason behind this is related to the role of thermal and mechanical strains. At an early stage (Case 1 of Fig. 6.9a), the ground surface is subjected to mechanical stretching strains higher than those of thermal origin together with constraints from deep layers. Therefore a tensile stress is developed. In later stages (Case 2 and Case 3 in Fig. 6.9a), the mechanical strains become much less than the thermal strains, which in turn forces the ground surface to expand and thus a compressive surface stress develops. The plane stress σ_{yy} remains tensile due to the dominant effect of mechanical shear strains caused by the horizontal grinding force (see Fig. 6.9b). It is clear that both the stress components vanish as the traction moves away.

For a deeper understanding of the above mechanism, the residual stresses induced by sole sources, i.e. by only mechanical or thermal deformation, are compared with those due to the coupled effect, as illustrated in Fig. 6.10. The thermal residual stresses are tensile. But the sole mechanical residual stresses are negligible compared with the thermal. However, the coupling of mechanical deformation with thermal deformation results in a residual stress free state. This clearly indicates that the coupling is very non-linear.

An increase of table speed results in a higher material removal and consequently generates a higher heat input. When table speed is sufficiently large, more heat is diffused in the direction of grinding which in turn results in a more localized temperature rise in the

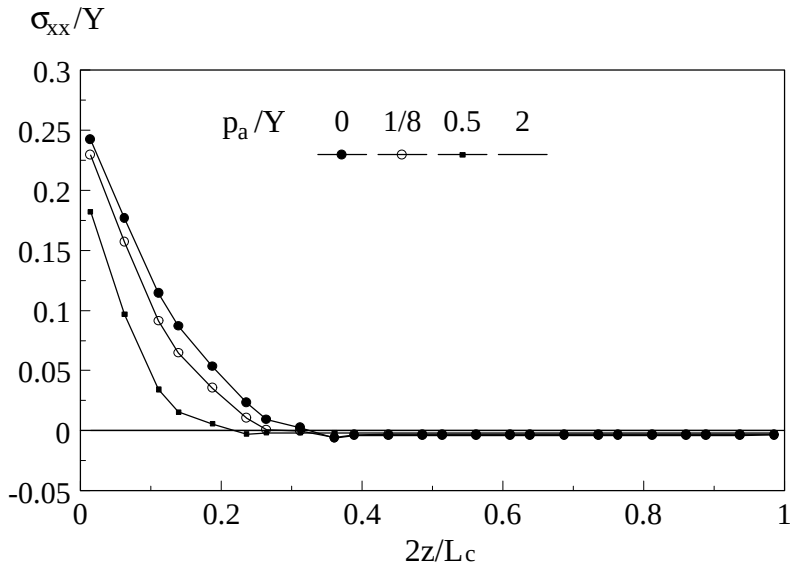

(a) σ_{xx}

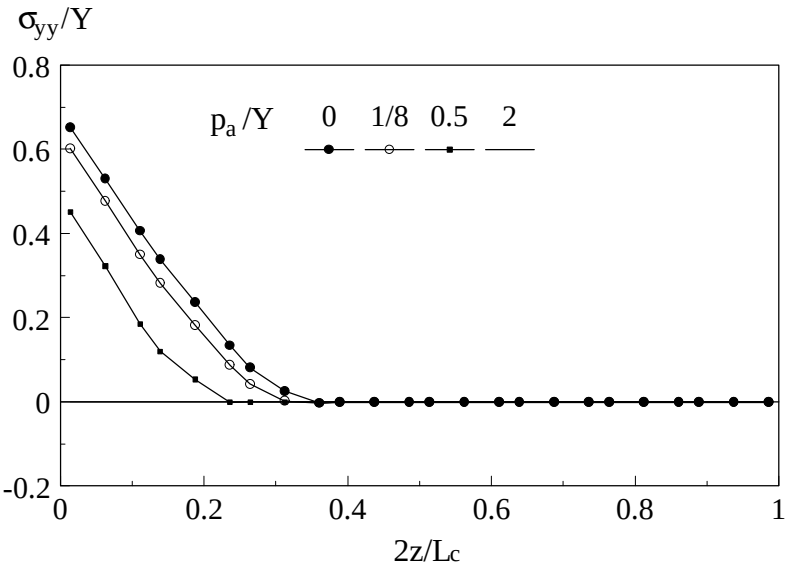

(b) σ_{yy}

Fig. 6.8 Cooling effect on residual stresses distributions
(H=1.0, l_a =0.25, Pe=1, q_a =43.25MW/m^2, μ=0.1)

vicinity of the workpiece surface but reduces the maximum grinding temperature. Figure 6.11 shows that the effect of increasing the table speed and the convection heat transfer coefficient has similar influence on residual stresses with coupled thermal-mechanical properties.

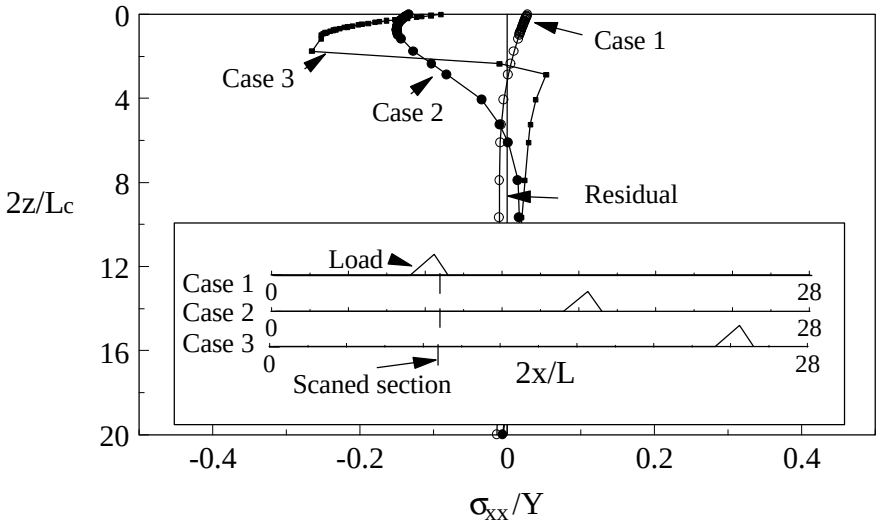

(a) σ_{xx}

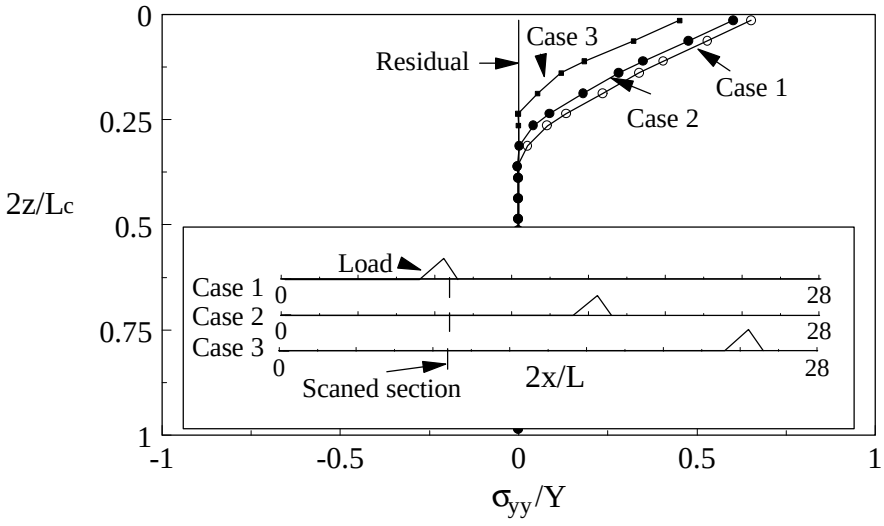

(b) σ_{yy}

Fig. 6.9 Thermo-mechanical stress history

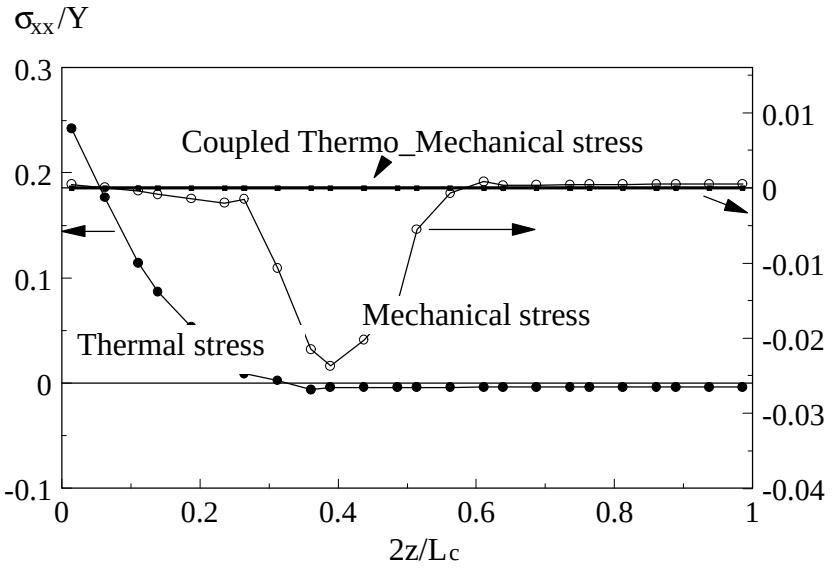

(a) σ_{xx}

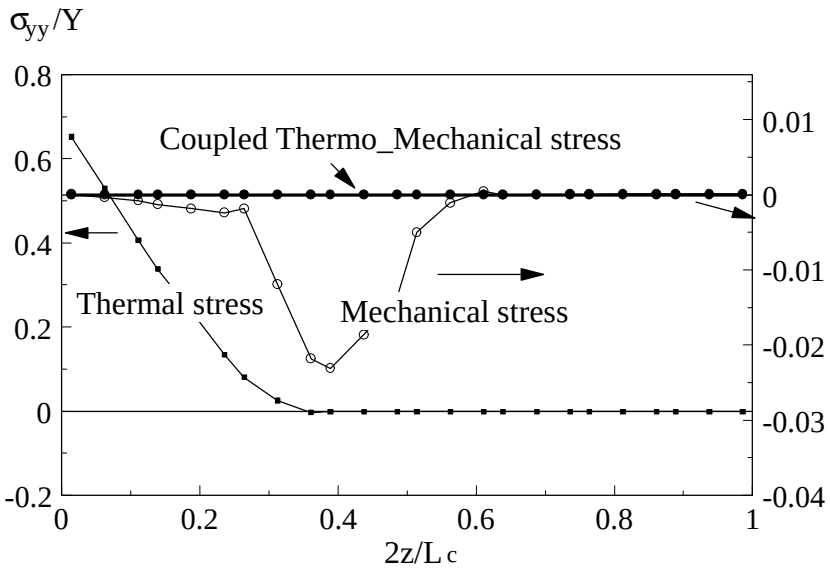

(b) σ_{yy}

Fig. 6.10 Coupling mechanism

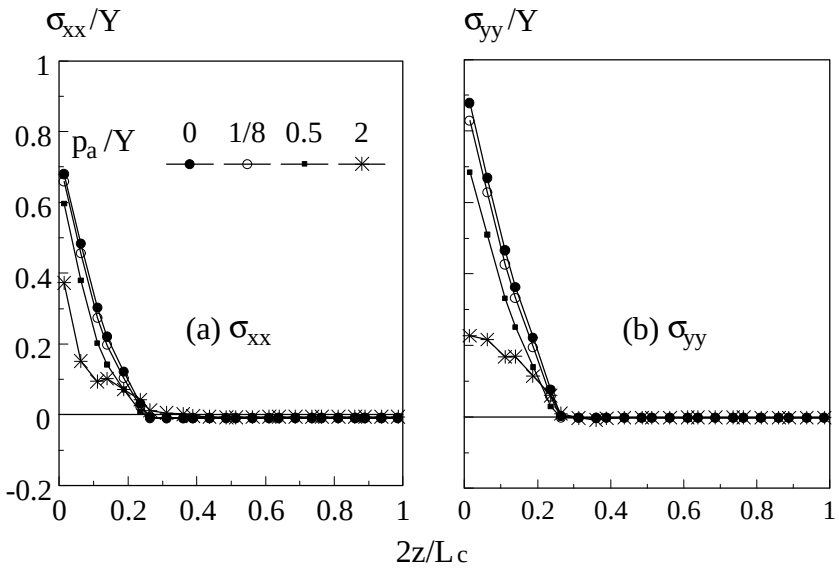

Fig. 6.11 The table speed effect
(H=0.0, l_a =0.25, Pe=4, q_a =47.25 MW/m^2 , μ=0.1)

6.4 Thermo-Mechanical Residual Stresses with Phase Change

When a workpiece experiences a critical temperature variation in grinding, phase change occurs at a certain distance away from the grinding zone as demonstrated by Fig. 6.12 It is clear that phase change starts earlier if the coefficient of convection heat transfer, H, is higher, regardless of the variation of table speed, which is reflected by a change of the Peclet number, Pe. Moreover, less cooling in the grinding zone ($0 \le w < 1$) accelerates the initiation of phase transformation if H is high, for instance, H = 1.

The variation of grinding conditions does not affect the two major surface residual stresses, σ_{xx} and σ_{yy}, when phase transformation occurs, as shown in Fig 6.13. The residual

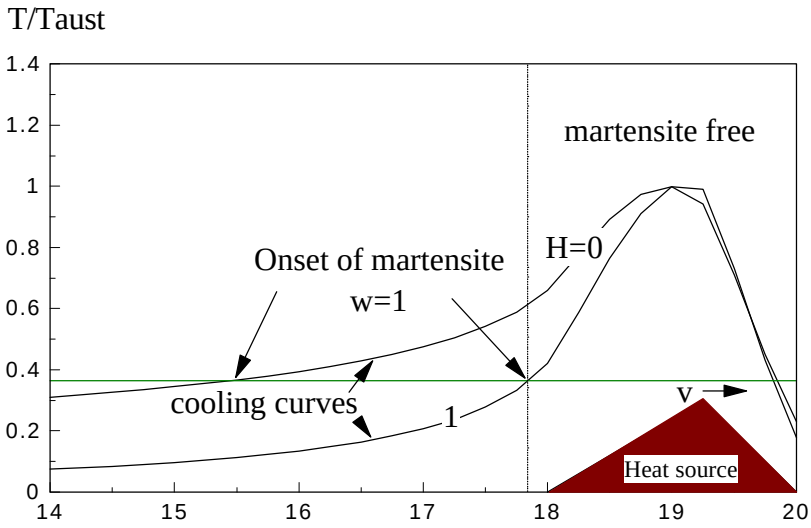

(a) Pe=1

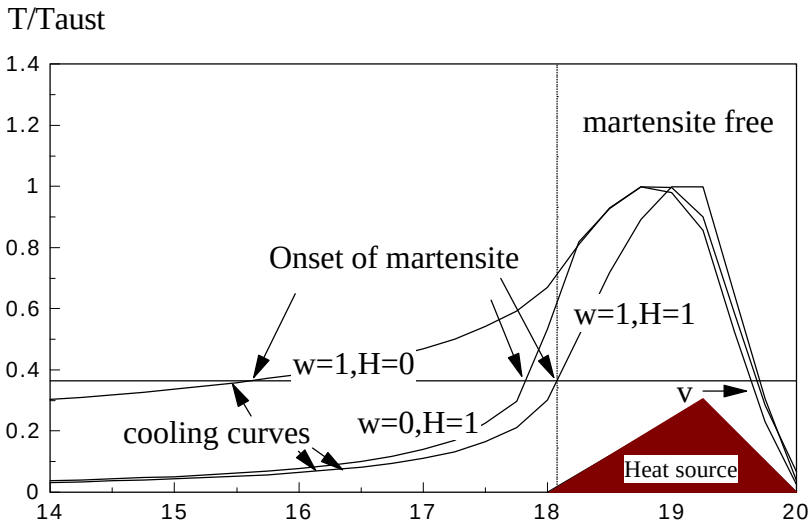

(b) Pe=1

Fig. 6.12 Onset of phase change vs heat source location (l_a=0.25)

stress σ_{yy} is nearly constant across the martensite zone (Fig. 6.13b,c). The longitudinal residual stress σ_{xx}, however, changes linearly, with a limit, within the martensite zone. At the boundary of the martensite zone, a rapid change of residual stresses occurs due to the sudden change of workmaterial properties. Compared with σ_{yy}, σ_{xx} is more affected by the type of grinding

operation, the ratio of horizontal to vertical forces and the fully coupled thermo-mechanical grinding conditions with phase change. The maximum σ_{xx} and σ_{yy} are 1.5 and 2.6 times higher, respectively, than the initial yield stress of the workmaterial, Y, and they are tensile at the ground surface. These characteristics are similar to those of purely thermal residual stresses without phase change as discussed in our previous study [Mahdi and Zhang (1997a)]. However, the coupling of phase transformation with thermal and mechanical deformation brings about much higher tensile residual stresses at the workpiece surface.

The coupling of mechanical loading with thermal loading and phase transformation has a minor influence on residual stress distribution for a wide range of magnitude of surface traction, as shown in Fig. 6.14. Moreover, at a higher ratio of horizontal to vertical traction, e.g. $\mu = 0.3$ (Fig. 6.14b), the increase of traction slightly decreases the longitudinal surface residual stress, σ_{xx}. The reason behind that is related to the reduction of the longitudinal strain within the grinding zone. As shown in our previous investigation [Mahdi and Zhang(1996b)], a higher mechanical traction with a down-grinding produces less longitudinal tensile residual stresses. However, associated with high mechanical traction, thermal strains become considerably higher and strains due to phase transformation also contribute remarkably to the workpiece deformation. Thus compared with thermal deformation and phase transformation, the effect of mechanical traction becomes minor. In the case of martensite phase transformation, the strains at the austenising grinding temperature play a central role in the formation of tensile residual stresses.

An up-grinding (e.g., $l_a = 0.25$) would result in a slightly deeper hardened layer compared with a down-grinding (e.g., $l_a = 0.75$), as shown in Fig 6.15. This is reasonable because an up-grinding operation produces a higher grinding temperature if other conditions are the same. Furthermore, the depth of the zone with large residual stresses is directly related to the thickness of the hardened martensite layer that is characterized by a higher martensite yield stress, $(\sigma_y)_m$, about 2.8 times the original yield stress, Y, of the workmaterial, as illustrated in Fig. 6.16. It is interesting to note that although the hardened layer thickness decreases as the input of grinding heat flux decreases, the level of maximum

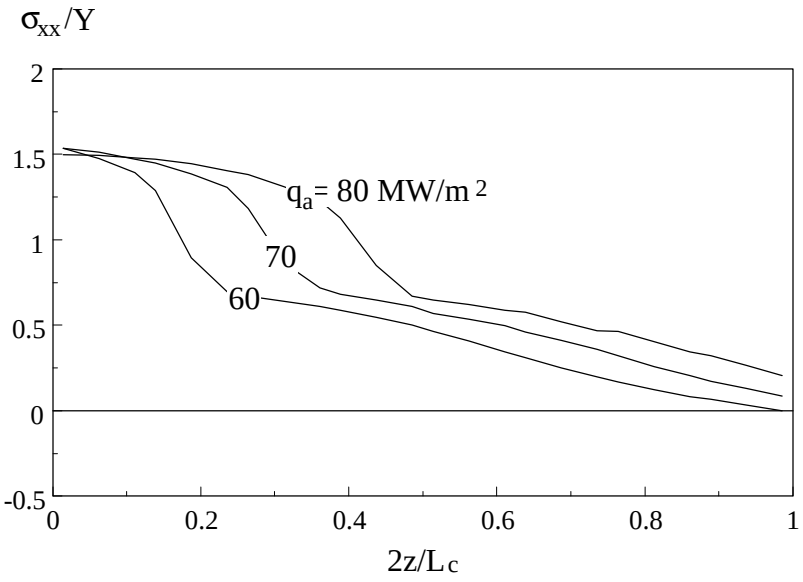

(a) σ_{xx},(Pe=1)

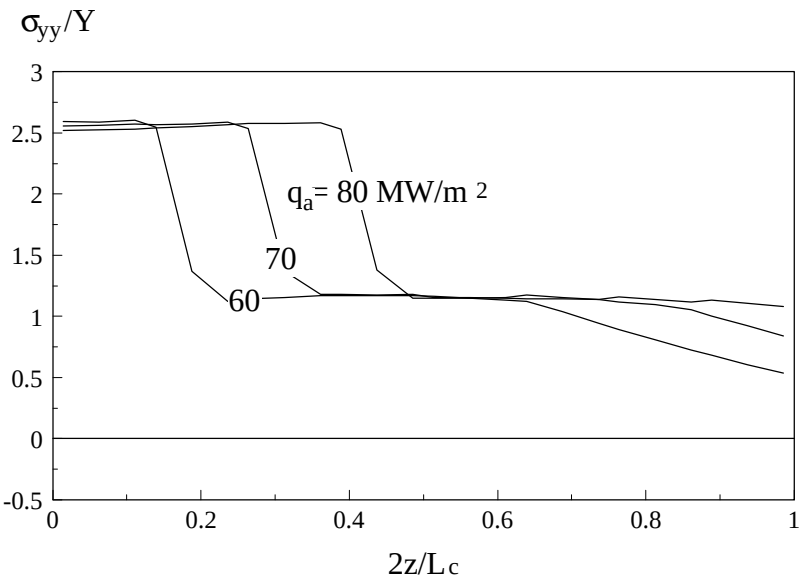

(b) σ_{yy},(Pe=1)

Fig. 6.13 Thermal residual stresses without surface cooling (H=0,l_a=0.25)

residual stresses in the martensite zone does not change. For a down-grinding process, similar dependence of residual stresses on the depth of the martensite zone exists.

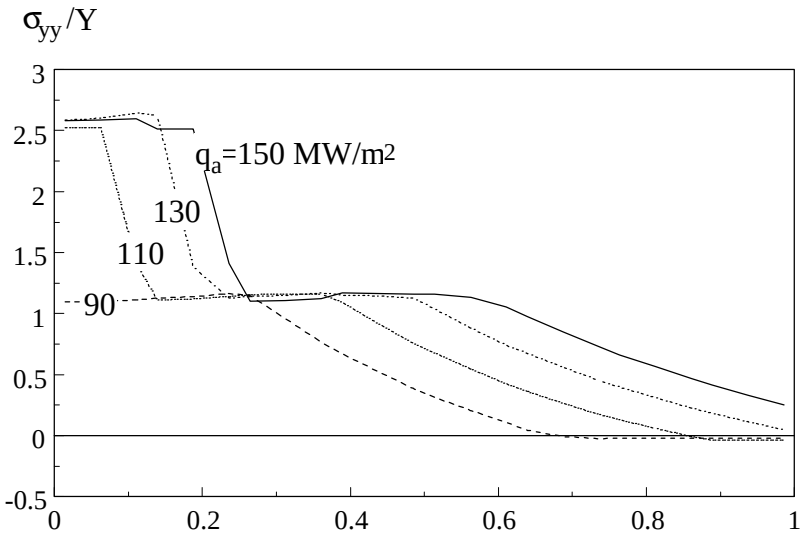

(c) σ_{yy},(Pe=4)

Fig. 6.13 Thermal residual stresses without surface cooling ($H=0, l_a=0.25$) (continued)

The Peclet number of a grinding process, Pe, reflects the variation of the grinding table speed and thus the thermal energy diffusion rate through the ground surface. An increase of Pe results in a decrease of grinding temperature and an increase of cooling rate, if all the other grinding conditions are the same. Therefore to maintain the same grinding temperature and martensite depth a higher input of heat flux is needed compared with the cases of Fig. 6.16. Figure 6.17 demonstrates the power of a cooling mechanism on residual stress distributions. It is clear that no-cooling inside the grinding zone (i.e., w = 0) would decrease greatly the required heat flux to generate the same martensite depth. Moreover, the thickness change of the martensite layer is more sensitive to the change of the input heat flux when w = 0 (Fig. 6.17b). Compared with the residual stresses associated with a low table speed, (e.g., Pe = 1), a high table speed (e.g., Pe = 4) would increase slightly the maximum surface residual stresses if phase change occurs. This is attributed to the higher yield stress of martensite associated with a higher Pe and a larger H, as indicated by Fig. 6.18.

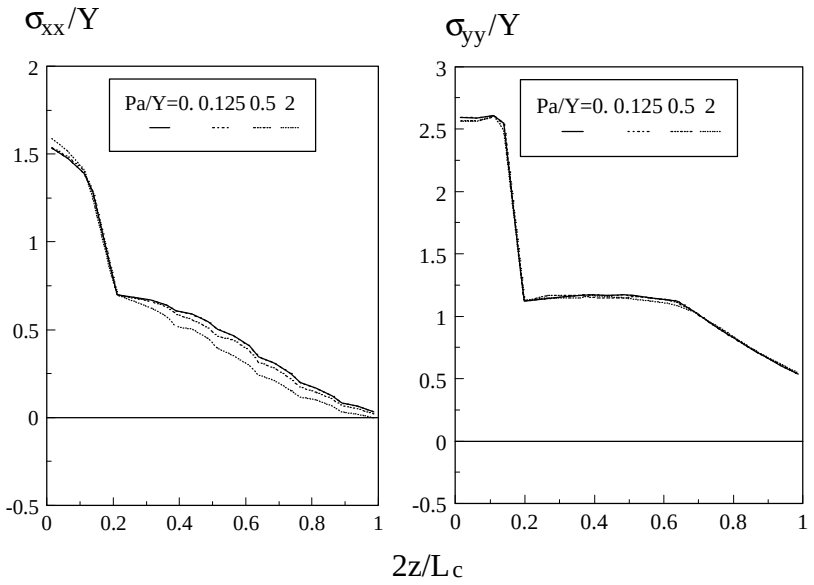

(a) μ=0.1

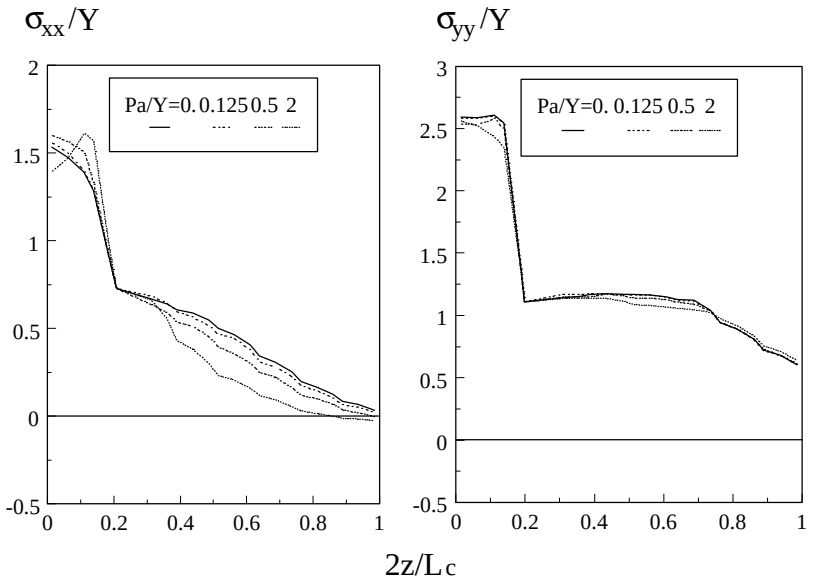

(b) μ=0.3

Fig. 6.14 The effect of mechanical traction on residual stress ($H=0$, $l_a=0.25$, $Pe= 1$ and $q_a =60$ MW/m^2)

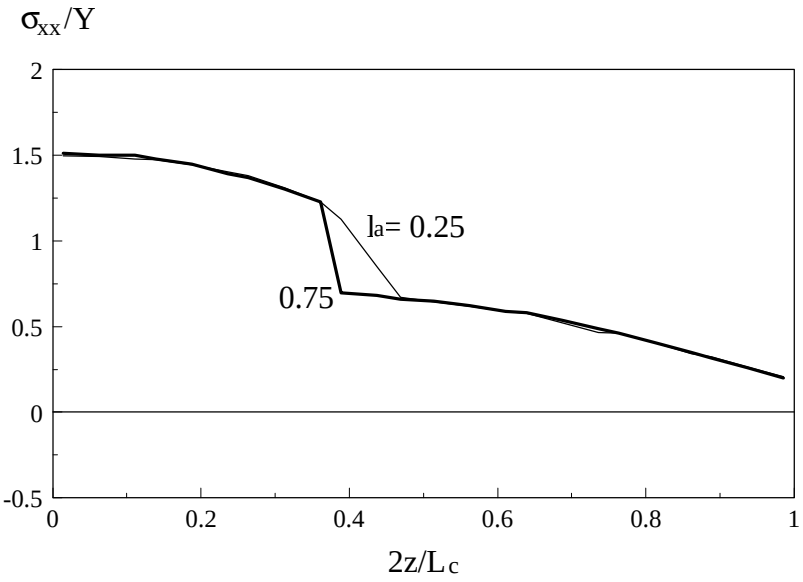

(a) σ_{xx}

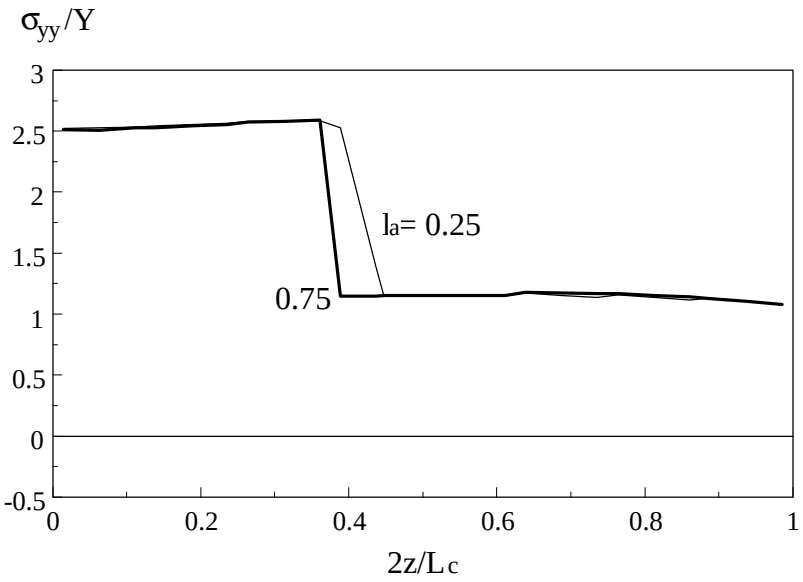

(b) σ_{yy}

Fig. 6.15 The effect of grinding type on residual stress ($H=0$, $p_a=0$, $Pe= 1$ and $q_a =60$ MW/m^2)

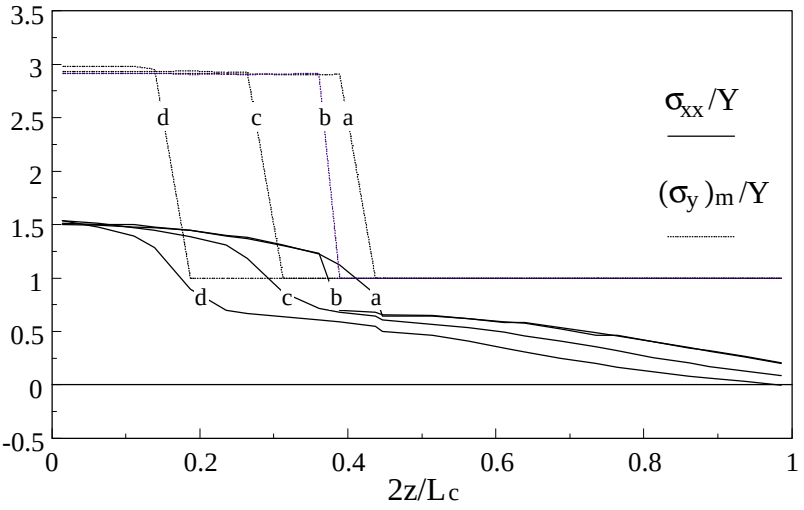

Curve a: l_a=0.25, q_a =80 MW/m^2 Curve b: l_a=0.25, q_a =70 MW/m^2

Curve c: l_a=0.25, q_a =60 MW/m^2 Curve d: l_a=0.75, q_a =70 MW/m^2

Fig. 6.16 Martensite yield stress, σ_y and the residual stress in grinding direction, σ_{xx}(H=0, Pe=1, p_a=0)

The effect of grinding conditions on the nature of residual stresses can be understood more deeply by comparing the influence of the causes individually and with different combinations. Figure 6.19 shows the role of each mechanism of different grinding conditions on longitudinal residual stress, σ_{xx}. Under sole mechanical conditions (case 1), a very small, almost negligible, residual stress is developed. Sole thermal grinding conditions without surface hardening (case 2) lead to a tensile residual stress, which decreases gently with subsurface depth. When phase transformation (surface hardening) is coupled, however, (see case 3), a surface layer with a greater tensile residual stress is generated. The variation of σ_{xx} also becomes sharper compared with case 2. By coupling the mechanical grinding conditions of case 1 with those of case 3, a considerable decrease in residual stress occurs, see case 4. It means that mechanical grinding conditions may have stronger effects on residual stresses when combined with thermal conditions only, particularly at a lower Pe. This is similar to the results of thermo-mechanical grinding conditions when the workmaterial properties are temperature-independent [Mahdi and Zhang(1998d)].

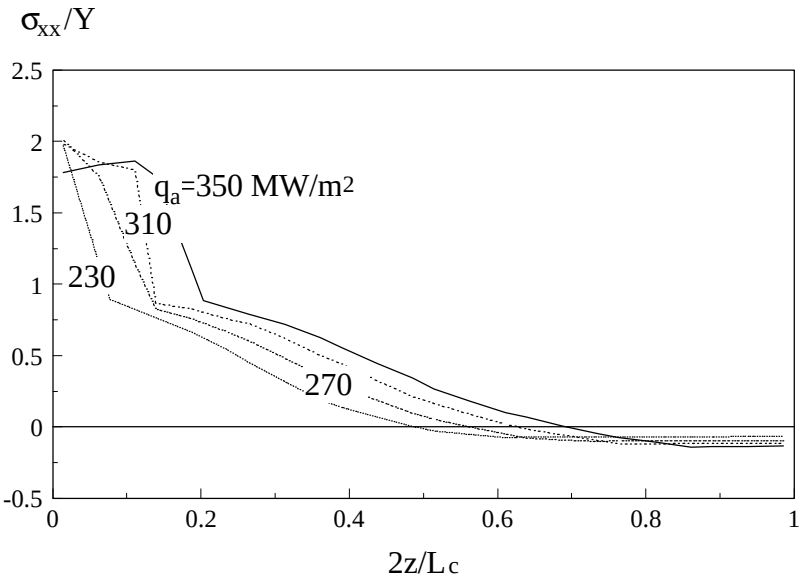

(a) w=1

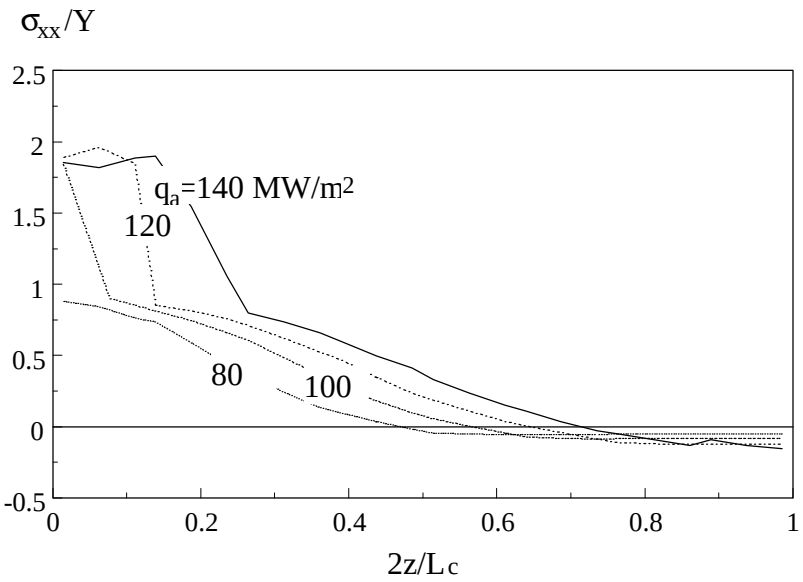

(b) w=0

Fig. 6.17 The effect of cooling on thermal residual stresses (H=0, Pe=1, l_a=0.25)

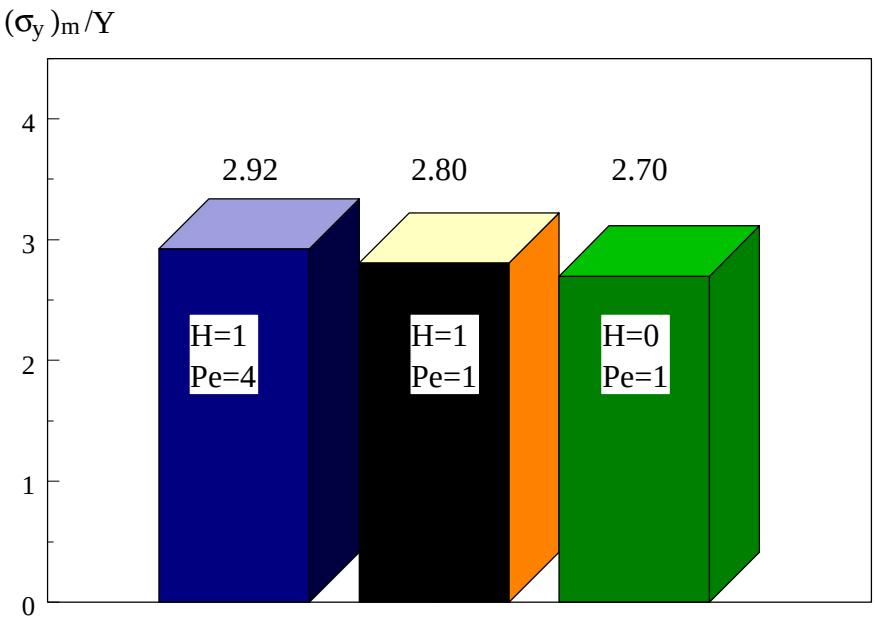

Fig. 6.18 Martensite yield stress (l_a=0.25, Tmax= T

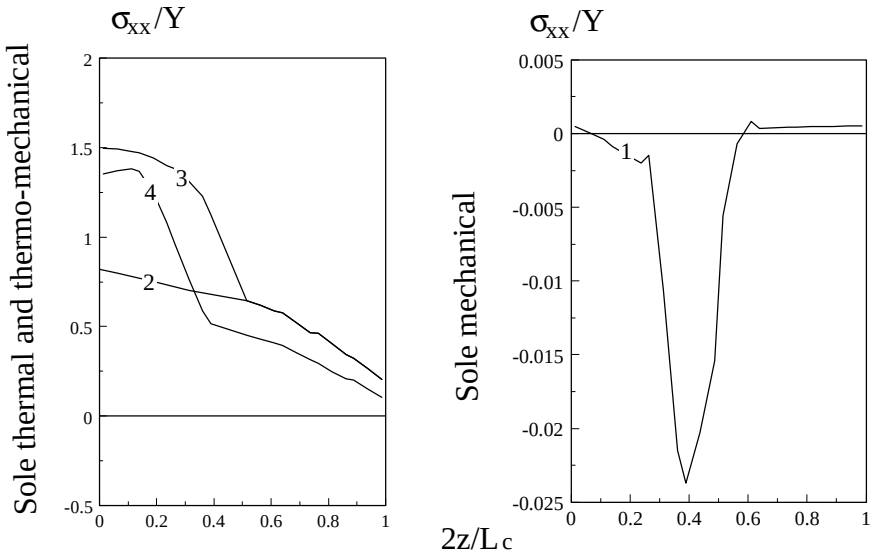

Case 1: p_a=2, μ =0.1
Case 2: l_a=0.25, q_a=80 MW/m^2 , Pe=1, H=0
Case 3: Case 2 coupled with phase transformation
Case 4: Case 3 coupled with Case 1

Fig. 6.19 Effect of individual grinding conditions

6.5 Summary

This chapter combined the effect of all factors in residual stress mechanisms. The onset of critical thermo-mechanical grinding conditions were investigated. To explore the coupling mechanism of thermal and mechanical grinding parameters, surface strain and stress histories were monitored. The development of thermo-mechanical residual stresses under some typical grinding conditions was thoroughly explored. The effects of phase transformation on residual stress were also taken into account.